# Tensile Analysis of TIG Welded Steel Rods with Varying Joint Angles

**Jitendra Amrute**

**ABSTRACT**

Welding is one of the most widely used joining processes in structural and mechanical applications, where joint configuration plays a critical role in determining the mechanical performance of welded components. In the present work, an experimental investigation is carried out to study the tensile behavior of TIG welded mild steel rods with varying joint angles. Five mild steel specimens of equal dimensions were prepared with joint angles of 0° (horizontal), 15°, 30° and 45°. The specimens were joined using Tungsten Inert Gas (TIG) welding under similar welding conditions to ensure consistency.

Tensile testing was performed on all welded specimens using a Universal Testing Machine (UTM) to evaluate load carrying capacity, deformation behavior, and failure characteristics. Load–displacement data obtained during testing was used to plot stress–strain curves for comparative analysis. The experimental results indicate that joint angle has a significant influence on tensile strength and ductility of welded joints. The horizontal (0°) joint exhibited the highest ductility and stable fracture behavior, while inclined joints showed reduced elongation due to stress concentration effects. Higher joint angles induced combined shear and bending stresses, leading to premature failure, predominantly near the weld metal and heat affected zone (HAZ).

The study concludes that lower joint angles provide better stress distribution and improved tensile performance in TIG welded mild steel rods. The findings of this research are useful for optimizing joint design in welded structures subjected to tensile loading and provide a basis for further investigations involving fatigue behavior, microstructural analysis, and numerical simulation.

**Keywords:** TIG Welding, Mild Steel, Joint Angle, Tensile Test, Stress–Strain Behavior, UTM, Weld Zone, HAZ

## CHAPTER 1
## INTRODUCTION

### 1.1 General Introduction

Welding represents a fundamental fabrication technique within mechanical and structural engineering, serving as a permanent method for uniting metal components through the application of heat, pressure, or a combination of both. Of the numerous welding methods available, Tungsten Inert Gas (TIG) welding is frequently selected for applications demanding superior joint quality.

Across diverse engineering structures including pressure vessels, pipelines, frameworks, and machinery welded connections often experience tensile forces. Consequently, analysing the tensile performance of these joints is essential for ensuring safe and reliable design.

### 1.2 Welding

Welding is a permanent joining technique where two or more metal components are fused by applying heat, pressure, or a combination of the two. This process may involve a filler material and results in a robust metallurgical bond. During welding, the base metals at the joint either melt or become plastic, eventually solidifying to create a unified structure.

#### 1.2.1 Classification of Welding Processes

Welding techniques are primarily categorized according to their source of heat, application of pressure, and mechanism of fusion.

#### 1.2.2 Fusion Welding (Non-Pressure Welding)

In this category of processes, the base metals are melted at the intended joint without the application of external pressure.

These methods are employed when strong, permanent bonds are necessary.

- Gas Welding
- Arc Welding

### 1.2.3 Solid-State welding (pressure welding)

The category of processes joins base metal without melting them utilizing applied pressure, something in combination with heat. These methods typically result in joints with minimal distortion and no distinct heat-affected zone.

### 1.2.4 Gas Welding

This method employs a gas flame as the primary heat source. It is commonly applied to thin sheets, repair operations, and pipeline work.

- Oxy-acetylene Welding
- Oxy-hydrogen Welding

### 1.2.5 Arc Welding

This process utilizes an electric arc formed between an electrode and the workpiece to produce the necessary heat. It is the most extensively used welding technique in industrial settings.

### 1.2.6 Resistance Welding

Heat in this method is generated by the electrical resistance at the joint interface, combined with applied pressure. It is prevalent in the automotive and sheet metal fabrication industries.
Examples include:

### 1.2.7 Special Welding Processes

These are advanced techniques designed for high-precision applications, frequently used in aerospace, nuclear, and medical industries.
Examples include:

## 1.3 Types of Welding

Welding is categorized into various types depending on the source of heat, the application of pressure, and the specific technique employed.

### 1.3.1 Gas welding

The described process is oxy-acetylene welding, a gas welding technique where metals are joined using heat generated by the combustion of acetylene with oxygen. A flame temperature reaching approximately 3200°C is produced, capable of melting most ferrous and non-ferrous metals. In this process, the base metal and a filler rod are fused together to create the joint. This method is primarily utilized for thin sheets, pipe welding, and repair tasks due to its excellent control over heat input. However, it is a relatively slow process and is generally not recommended for joining thick sections of material.

### 1.3.2 Arc welding

The described process is arc welding, a method where heat is generated by an electric arc established between an electrode and the workpiece. The extreme temperature of the arc, which can approach 6000°C, melts both the base metal and the electrode to form a robust joint. Arc welding is extensively employed in industrial settings owing to its high efficiency and adaptability.

### 1.3.3 Gas Metal Arc Welding (MIG/GMAW)

The described process is Gas Metal Arc Welding (GMAW), commonly known as MIG (Metal Inert Gas) welding. This arc welding technique employs a continuously fed solid wire electrode and an external shielding gas, typically argon, carbon dioxide, or a mixture. The consumable wire serves as both the electrode and the filler metal. MIG welding is

known for producing clean, high-integrity welds at a high deposition rate. It is extensively used in automotive and general manufacturing sectors, particularly for joining thin to medium-thickness materials.

### 1.3.4 Gas Tungsten Arc Welding (TIG/GTAW)

The described process is Gas Tungsten Arc Welding, commonly known as TIG (Tungsten Inert Gas) welding. This arc welding method utilizes a non-consumable tungsten electrode to generate the arc. A separate filler rod can be introduced if needed, and an inert shielding gas such as argon is used to protect the weld zone from atmospheric contamination. TIG welding offers superior control and produces high-quality, clean welds with minimal defects. This makes it ideal for welding materials like stainless steel and aluminum, as well as for fabricating critical components in the aerospace and nuclear industries.

### 1.3.5 Submerged Arc Welding (SAW)

The described process is Submerged Arc Welding (SAW). This arc welding technique submerges both the arc and the molten weld pool beneath a blanket of granular flux. This flux layer shields the weld from atmospheric gases and enhances overall weld integrity. SAW is typically performed as an automatic or semi-automatic operation and is extensively used for joining thick sections in applications such as shipbuilding, pressure vessel fabrication, and the construction of heavy structures.

### 1.3.6 Thermit welding

The process is Thermit Welding This technique utilizes heat produced by an exothermic reaction between aluminum powder and a metal oxide, typically iron oxide. The reaction generates molten iron, which is directed into a prepared joint where it solidifies to create the weld.

### 1.3.7 Plasma arc welding

The process is Plasma Arc Welding This advanced welding method utilizes a constricted arc created by ionized gas, known as plasma, to generate extremely high temperatures. It enables deep weld penetration with superior precision and control. Plasma Arc Welding is employed for high-integrity and critical applications, especially within the aerospace sector, for stainless steel fabrication, and in other advanced manufacturing industries.

### 1.3.8 Laser beam welding

The described process is Laser Beam Welding. This advanced technique utilizes a highly focused, coherent laser beam as an intense heat source to fuse metals. It produces a very narrow weld seam with a minimal heat-affected zone and operates at exceptionally high speeds. Laser welding is widely implemented in industries demanding high precision, such as electronics, medical device manufacturing, and automotive production.

### 1.3.9 Electron beam welding

The described process is Electron Beam Welding. This is a high-energy fusion welding technique that utilizes a focused beam of high-velocity electrons to generate intense heat at the joint. The operation is typically conducted within a vacuum chamber to prevent the scattering of electrons by air molecules. Electron Beam Welding is characterized by its deep penetration capabilities, excellent weld integrity, and minimal thermal distortion. It is predominantly employed in high-tech sectors such as aerospace, nuclear engineering, and other fields requiring extreme precision.

## 1.4 Tensile Test

A tensile test is a fundamental mechanical evaluation performed to ascertain the strength and deformation characteristics of a material under an axial pulling force. For this test, a standardized specimen is securely gripped at both ends within a testing machine and is steadily elongated until it breaks. The procedure reveals the material's response to tension and identifies the maximum safe load it can endure prior to failure.

During the test, a progressively rising axial force is applied, causing the specimen to extend. Initially, the material experiences elastic deformation, meaning it would return to its original dimensions if unloaded. Once the applied load

surpasses the elastic limit, the material enters the plastic deformation phase, where permanent stretching occurs. The test concludes with fracture at the specimen's weakest point.

A tensile test is typically conducted using a Universal Testing Machine (UTM). The outcomes are commonly presented as a stress-strain curve, which illustrates the correlation between the applied stress and the resulting strain. This test is extensively applied in quality assurance, research and development, and engineering design to verify that materials comply with necessary strength and safety criteria.

### 1.4.1 Tensile Test Procedure

The tensile test is conducted on a Universal Testing Machine (UTM) to assess a material's mechanical behavior under axial tension. The procedure begins with the preparation of a standard tensile specimen, which is machined according to specifications from standards like ASTM or IS codes. This specimen features a uniform cross-section within its gauge length to promote even stress distribution during loading.

Following preparation, key specimen dimensions—such as the original gauge length and cross-sectional diameter or width—are precisely measured using tools like a vernier caliper or micrometer. These initial measurements are essential for subsequent stress and strain calculations. The specimen is then firmly clamped between the upper and lower grips of the UTM, with careful alignment to prevent any bending or eccentric loading.

With the specimen secured, a tensile load is applied along its axis at a constant, controlled rate. As the force increases, the specimen elongates. In the initial stage, this elongation is minimal and directly proportional to the load. The UTM's data acquisition system continuously logs the applied load and the corresponding extension.

Upon further loading, the material reaches its yield point, marking the onset of permanent plastic deformation. Continued loading leads to necking, a localized contraction of the cross-section. The test concludes when the specimen fractures at its weakest point. The machine is then halted, and the fractured pieces are retrieved.

Post-test measurements of the final gauge length and the reduced cross-sectional area at the neck are taken. These values are used to compute the percentage elongation and percentage reduction in area, which are critical for determining the material's key mechanical properties.

### 1.5 Tensile Test of Welded Joints

A tensile test on a welded joint is conducted to assess the strength and integrity of the weld relative to the parent metal. For this evaluation, a specimen is prepared with the weld positioned within its gauge length, typically encompassing the weld metal, the heat-affected zone (HAZ), and the base metal.

The welded specimen is installed in a Universal Testing Machine following the standard procedure for a tensile test. An axial tensile load is applied progressively until the specimen ruptures, with both the applied force and corresponding elongation being recorded throughout the process.

The tensile strength of the welded joint is determined by dividing the maximum load sustained by the specimen's original cross-sectional area. This test is crucial in welding applications as it aids in evaluating how key welding variables—such as current, voltage, travel speed, and joint geometry—affect the mechanical performance of the welded connection.

### 1.6 Universal Testing Machine (UTM)

A Universal Testing Machine (UTM) is a versatile mechanical testing apparatus designed to assess material properties by imposing regulated tensile, compressive, flexural, or shear forces. It earns the designation "universal" because a single unit can conduct a variety of evaluations—including tensile, compression, bending, and shear tests—and, with appropriate accessories, certain fatigue-related assessments. The UTM precisely measures the applied load, deformation, and displacement, enabling the determination of key characteristics such as ultimate tensile strength, yield strength, percentage elongation, and elastic modulus.

### 1.7 Working Principle of UTM

The operating principle of a Universal Testing Machine (UTM) relies on applying a progressively increasing force to a test specimen while concurrently measuring the induced deformation. The specimen is secured within the machine's grips or between its platens, and the load is exerted by a moving crosshead. The magnitude of this force is quantified using a load cell or proving ring, while the specimen's extension or compression is tracked via an extensometer or a crosshead displacement sensor. The machine logs the force and deformation data continuously until the specimen fails or the predefined test conclusion is reached.

**Figure 1.1 Universal Testing Machine (UTM) Working Principle**

### 1.8 Classification of Universal Testing Machine

Universal Testing Machines are categorized according to their load application mechanism, control system, and load-bearing capacity.

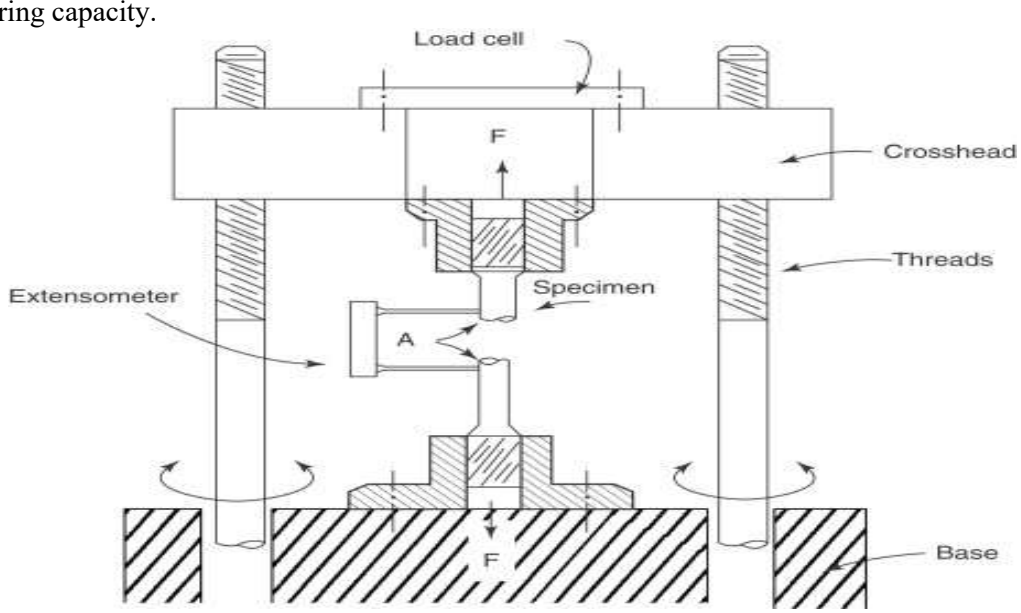


#### 1.8.1 Classification Based on Load Application System

Based on the mechanism for applying force to the specimen, Universal Testing Machines are divided into two primary types: mechanical and hydraulic.

A mechanical UTM exerts force through a system of screws, gears, and levers. A motor drives a movable crosshead via a screw mechanism, applying the load incrementally. These machines are typically employed for low to medium load capacities and offer reliable accuracy for standard laboratory testing. Their main limitations are slower operation and an inability to handle extremely high loads.

A hydraulic UTM generates force using hydraulic pressure produced by a pump, which is then transmitted through a piston and cylinder assembly. These systems can apply very high forces and are extensively used for testing large specimens like steel bars, plates, and structural members. Due to their high load capacity and smooth force application, hydraulic UTMs are prevalent in industrial testing facilities.

#### 1.8.2 Classification Based on Control System

Based on the control methodology and data acquisition system, Universal Testing Machines are categorized into manual, semi-automatic, and computerized (digital) types.

A manual UTM necessitates that the operator manually controls the load application and records the readings. These machines are primarily found in basic educational laboratories and offer lower precision compared to contemporary automated systems.

A semi-automatic UTM incorporates partially automated load application and features a digital display for load and

displacement. While some functions remain under operator control, this type improves data accuracy and repeatability. A computerized or digital UTM is fully automated and managed by dedicated software. It automatically records load, displacement, and stress-strain data, and can generate test graphs and reports. Due to their superior accuracy and efficiency, computerized UTMs are extensively used in research, quality assurance, and advanced materials testing.

### 1.8.3 Main Components of a Universal Testing Machine

A Universal Testing Machine comprises several key components that function together to conduct material tests. The load frame offers a sturdy, rigid structure to maintain proper alignment during testing. The movable crosshead travels vertically to apply tensile or compressive force to the specimen. Grips and fixtures securely clamp the specimen in place. The load measuring system, typically a load cell or proving ring, precisely quantifies the applied force. An extensometer or other displacement sensor measures the specimen's elongation or compression. In computerized systems, a control panel and software manage test execution and automatically record all data.

### 1.8.4 Applications of Universal Testing Machine

The Universal Testing Machine is extensively utilized in material testing laboratories, manufacturing sectors, construction, and research organizations. Its applications include performing tensile tests on metals and welded joints, compression tests on concrete and polymers, bending tests on beams, shear tests on fasteners, and general quality assurance for engineering materials. UTMs are essential for verifying material safety, performance, and adherence to established engineering standards.

### 1.8.5 Advantages of Universal Testing Machine

The primary advantage of a Universal Testing Machine is its versatility, as a single apparatus can conduct various types of mechanical tests. It delivers precise and dependable outcomes and is adaptable for evaluating a broad spectrum of materials. Contemporary computerized UTMs further minimize human error and enhance efficiency by automating data collection and report generation.

## CHAPTER 2:

## LITERATURE REVIEW

**[1] Elangeswaran et al.** examined the fatigue behavior of 316L stainless steel fabricated using Laser Powder Bed Fusion (LPBF). Their study focused on the influence of post-processing treatments such as stress-relief heat treatment and surface machining. The fatigue tests, conducted under fully reversed loading conditions, showed that surface machining greatly enhances fatigue life by removing surface defects and reducing stress concentration. Stress-relief treatment was found to improve fatigue consistency by minimizing internal residual stresses. Additive manufacturing has emerged as an advanced manufacturing route for producing stainless steel components with complex geometries.

**[2] Liu et al** Surface modification techniques are widely used to enhance the fatigue performance of stainless steels. studied the influence of low-temperature gaseous carburization on the fatigue behavior of AISI 316L stainless steel. Fully reversed axial fatigue tests revealed that carburization modifies the near-surface microstructure and induces compressive residual stresses, which delay crack initiation and slow down crack propagation. The study confirmed that surface-hardened layers play a vital role in improving fatigue resistance.

**[3] Sivasubramani et al.** reviewed the effect of friction welding and friction stir welding on the microstructure and fatigue behavior of duplex steel joints. Their analysis showed that refined grain structures formed in the weld zone enhance fatigue strength, while improved hardness distribution contributes to better notch sensitivity performance. The study highlighted the importance of welding parameters in achieving superior joint performance. Solid-state welding techniques have gained attention for joining duplex stainless steels due to their superior mechanical and corrosion properties**.**

**[4] Limbert et al.** emphasized that stainless steel reinforcement offers excellent corrosion resistance compared to conventional carbon steel reinforcement. Their work demonstrated that the mechanical behavior of reinforced concrete structures can be accurately predicted only when reliable constitutive models for stainless steel reinforcement are used. The study underlined the need for incorporating nonlinear material models in structural simulations. Corrosion-induced degradation of reinforcement steel is a major concern for concrete infrastructure.

**[5] Wood et al**.The fatigue performance of additively manufactured stainless steel is strongly influenced by build orientation and post-processing investigated the fatigue behavior of Selective Laser Melted steel fabricated in different orientations. Horizontally built specimens exhibited superior fatigue life compared to vertically built samples due to reduced anisotropy and defect sensitivity. Surface machining was found to significantly enhance fatigue resistance by eliminating near-surface imperfections.

**[6] Liu et al** Advanced surface engineering methods such as ultrasonic surface rolling have shown significant potential in improving fatigue lif. fabricated a gradient nanostructured surface layer on 17-4PH stainless steel using Ultrasonic Surface Rolling Process (USRP). The induced nanocrystalline structure and compressive residual stress improved fretting fatigue resistance by reducing surface damage and delaying crack nucleation.

**[7] Dai et al.** Laser Shock Peening (LSP) is another effective surface treatment for fatigue enhancement. studied the effect of LSP on rolling contact fatigue performance of 316 steel. The treatment generated deep compressive residual stress layers and increased surface hardness, which significantly enhanced fatigue life under cyclic rolling contact conditions.

**[8] Chen et al.** Austenitic stainless steels are increasingly used in seismic applications due to their excellent ductility and energy dissipation capacity. conducted low-cycle fatigue tests on S30408 stainless steel at high strain amplitudes. The results demonstrated stable hysteresis behavior, high ductility, and nonlinear stress-strain response, indicating superior seismic performance.

**[9] Liu et al.** The influence of surface nano structuring on fatigue behavior was further investigated by Liu et al. for 2205 duplex steel. Their work showed that ultrasonic surface rolling improved high cycle fatigue life by increasing surface strength and inducing martensitic phase transformation. However, in low cycle fatigue conditions, the presence of the hardened surface layer reduced fatigue life due to limited plastic deformation capacity.

**[10] Zulić et al.** Laser Shock Peening (LSP) has emerged as an effective surface treatment technique for improving the fatigue performance of additively manufactured metals. investigated the influence of LSP on the fatigue life of additively manufactured 316L stainless steel using a diode-pumped laser system and sacrificial protective layers. Their results showed that LSP treatment introduced high compressive residual stresses into the surface layer, significantly improving fatigue life compared to as-built samples. The study demonstrated the feasibility of diode-pumped laser systems for industrial LSP applications and highlighted their potential for enhancing the structural reliability of additively manufactured stainless steel components.

**[11] Alsmadi et al.** High-temperature components often experience combined creep and fatigue damage under cyclic loading. studied the low-cycle fatigue behavior of Alloy 709 at 750°C with tensile hold times to evaluate creep–fatigue interaction. Their results showed that increasing hold time accelerated crack initiation and growth, leading to a reduction in fatigue life. Fractographic analysis confirmed that fatigue dominated deformation at lower strain ranges without hold times, while creep contributed significantly when hold times were introduced. The study validated fatigue life prediction using the ASME linear damage summation rule.

**[12] Annan et al.** evaluated the hysteresis behavior of austenitic Grade 304L stainless steel plates subjected to large inelastic cyclic strains for buckling-restrained brace applications. Compared to conventional carbon steel, stainless steel exhibited higher ductility and greater strain hardening under monotonic loading. However, under cyclic loading, it

showed stronger cyclic hardening and comparatively shorter low-cycle fatigue life. The study provided important cyclic plasticity parameters for numerical modeling of seismic-resistant structures.

**[13] Tang et al.** Additive manufacturing processes often introduce surface irregularities that influence buckling and strength behavior. investigated the effects of post-manufacturing surface treatments such as turning and sandblasting on the compressive buckling strength of LPBF-manufactured thin cylindrical shells. Their experimental results revealed that turning significantly improved buckling strength by producing a smoother surface finish, whereas sandblasting provided only marginal improvement. Microstructural analysis linked these improvements to contour scanning effects during the printing process.

**[14] Hua et al.** Bimetallic steel bars are being developed to enhance the durability of reinforced concrete structures. studied the low-cycle fatigue characteristics of bimetallic steel bars consisting of a carbon steel core and steel cladding. Their results showed stable hysteresis behavior and increasing peak stress with increasing strain amplitude. A fatigue degradation model was developed to relate strength loss to plastic strain range and cycle count. Numerical simulations further demonstrated the influence of nonlinear mechanics and inelastic buckling on fatigue behavior.

**[15] Cruces et al.** Multiaxial fatigue behavior is a critical design consideration for many engineering components. analyzed the multiaxial fatigue response of 316 stainless steel under various biaxial stress states using different critical plane models. Among the evaluated models, the Liu II model provided the most accurate fatigue life predictions, while the Liu I model most effectively predicted failure plane orientation. The study highlighted the importance of selecting appropriate fatigue criteria for complex loading conditions.

**[16] Soyama et al.** compared the effects of shot peening and cavitation peening on the fatigue performance of SUS316L stainless steel. Their results indicated that shot peening provided longer fatigue life at higher stress levels due to higher induced compressive residual stresses, although this stress relaxed more rapidly during fatigue cycling. Cavitation peening showed slightly higher fatigue strength at lower stress levels. The study demonstrated that adjusted yield stress correlates well with fatigue performance.

**[17] Zou Yun et al.** investigated the influence of WJP on the mechanical and fatigue properties of 304 stainless steel at various treatment pressures. The results showed that treatment at 200 MPa produced an optimal hardened surface layer with high compressive residual stress, improved tensile strength, and enhanced ductility. These improvements were attributed to grain refinement, phase transformation, reduced surface roughness, and a favorable residual stress distribution.

**[18] Kumar et al.** Different additive manufacturing routes can produce stainless steel components with distinct microstructural and fatigue characteristics. compared the fatigue resistance and mechanical behavior of 316L stainless steel produced by Binder Jet Printing, Selective Laser Melting, and conventional manufacturing. Despite higher porosity, binder jet printed samples exhibited fatigue strength comparable to conventionally manufactured material due to a planar slip regime that arrested crack propagation at pores. In contrast, SLM samples showed lower fatigue life due to coarse columnar grain structures.

**[19] Lai et al.** Residual stresses play a critical role in determining fatigue performance of additively manufactured components. investigated the effect of residual stress on the fatigue strength of LPBF 316L stainless steel. Their results demonstrated that stress relief heat treatment significantly improved fatigue strength by eliminating tensile residual stresses present in as-built samples. However, when the stressed surface layer was removed through machining and polishing, heat treatment had little effect. The study emphasized the importance of residual stress control in fatigue-critical LPBF components.

**[20] Benchouia et al.** The fatigue performance of welded steel joints is strongly influenced by loading conditions and post-weld surface treatments. investigated the fatigue life of GTAW welded AISI 304L stainless steel under different stress ratios and after shot peening treatment. Their results showed that fully reversed loading conditions produced longer

fatigue life compared to tension–tension loading. Shot peening significantly improved fatigue resistance by increasing surface hardness and introducing beneficial compressive residual stresses, with peening duration playing a more dominant role in fatigue improvement than in hardness enhancement.

**[21] Braun et al.** Hybrid additive–subtractive manufacturing techniques are increasingly used to improve surface quality and mechanical performance of additively manufactured metals. examined the fatigue strength of AISI 316L stainless steel produced by laser powder bed fusion followed by machining and heat treatment. Their study revealed that machining dramatically increased fatigue strength by removing near-surface defects, while heat treatment further enhanced performance by relieving residual stresses. Computed tomography analysis helped determine the required machining depth for defect removal.

**[22] Krovvidi et al.**High-temperature components used in nuclear applications require reliable fatigue design data. generated comprehensive tensile and low-cycle fatigue data for SS316Ti at elevated temperature conditions. Their results showed that fatigue life decreases with increasing strain range and tensile hold periods. Based on the experimental data, design fatigue curves and cyclic stress–strain relationships were developed in accordance with ASME and RCC-MR design codes.

**[23] Jin et al.** Pre-strain conditions have a strong influence on fatigue performance of mild steels. investigated the effect of tensile and torsional pre-strains on the fatigue life of 304 stainless steel. Their results revealed a characteristic "S-shaped" relationship between pre-strain and fatigue life. The study also showed that torsional pre-strain induces higher internal stress compared to tensile pre-strain, leading to earlier initiation of martensitic transformation and fatigue damage.

**[24] De Abreu et al.** studied the failure behavior of lean duplex stainless steel wires under combined static and cyclic axial loading along with transverse loading. Their investigation established empirical fracture and endurance criteria and compared the results with conventional eutectoid steel wires. Microscopic analysis confirmed that loading mode strongly influences fatigue crack initiation and propagation mechanisms.

**[25] Farrahi et al.** Fretting fatigue is a major concern in mechanical assemblies subjected to combined bending and tensile loads. investigated the fretting fatigue behavior of 316L stainless steel using a specially designed experimental setup. Their results showed that increasing bending load contribution reduced stress concentration at contact edges and improved fretting fatigue life. Finite element analysis supported the experimental findings by predicting lower contact pressure and shear stress at critical locations.

**[26] Zhang et al.** studied the influence of grinding on the surface integrity and fatigue life of LPBF-fabricated 304L stainless steel. Their experimental results demonstrated that grinding significantly improved fatigue life by removing surface defects such as lack-of-fusion pores and keyholes. Microstructural analysis further revealed that grinding induces subsurface grain refinement, contributing to improved fatigue performance.

**[27] Liu et al**. investigated the fatigue response of additively manufactured 17-4PH stainless steel under combined axial and torsional loading. Their results showed that hot isostatic pressing effectively improves fatigue life by reducing internal porosity. Surface finishing further enhanced fatigue resistance by minimizing stress concentration at surface defects.

**[28] Jiang et al**. Residual stress evolution during cyclic loading has a strong influence on fatigue life of welded joints. developed a coupled residual stress–viscoelastic model to predict residual stress redistribution and its effect on fatigue performance of welded components. Their experimental validation confirmed that residual stress primarily affects fatigue life by increasing mean stress levels. A fatigue life prediction model incorporating residual stress was proposed and verified.

**[29] Huang et al.** Gradient nanostructured surface layers have shown exceptional capability in enhancing fatigue strength of stainless steels. fabricated a nanostructured surface layer on 316L stainless steel using surface mechanical rolling treatment. The treated material exhibited significantly higher fatigue strength in both low-cycle and high-cycle regimes. The improvement was attributed to suppression of crack initiation and enhanced accommodation of cyclic plastic strain within the nanostructured layer.

**[30] Li et al.** examined the performance of a newly developed stainless-steel-clad reinforcement bar intended for use in seismic-resistant concrete structures. Their work demonstrated that when conventional reinforced concrete members experience severe cyclic deformation, outer concrete layers tend to spall, exposing reinforcement bars to buckling and fatigue damage. To overcome this issue, a composite rebar consisting of a carbon steel core with stainless steel cladding was tested under combined buckling and low-cycle fatigue conditions. The results showed that the stainless-steel cladding significantly improves strength retention and fatigue life under cyclic deformation.

**[31] Elangeswaran** and co-workers investigated the fatigue characteristics of additively manufactured 316L stainless steel produced by laser powder bed fusion. Their study focused on minimizing internal porosity and achieving uniform microstructure by optimizing printing parameters. Fatigue testing under fully reversed loading conditions revealed that post-processing treatments such as stress relief and surface machining play a major role in determining fatigue strength and durability.

**[32] Liu and colleagues** studied the influence of low-temperature gaseous carburization on the surface properties of austenitic stainless steel. Their experimental results indicated that carburized layers with controlled case depth can significantly modify fatigue behaviour by improving surface hardness and residual stress distribution, thereby enhancing fatigue resistance under fully reversed loading.

**[33] Sivasubramani et al**. presented a comprehensive review on the fatigue behaviour of duplex steel joints produced using solid-state welding techniques such as friction welding and friction stir welding. Their analysis emphasized the relationship between microstructural evolution in the weld zone and mechanical performance, highlighting the importance of welding parameters in determining joint strength and fatigue endurance.

**[34] Limbert et al.** studied the long-term durability of stainless-steel reinforcement in concrete structures exposed to chloride-rich environments. Their findings confirmed that stainless steel reinforcement provides superior corrosion resistance compared to conventional carbon steel and offers improved structural reliability, especially in aggressive service conditions.

**[35] Wood and co-authors** analysed the effect of build orientation and post-processing on the fatigue performance of selective laser melted 316L stainless steel. Their results showed that horizontally fabricated specimens with surface machining exhibited the best fatigue behavior due to improved surface quality and reduced defect concentration.

**[36] Liu et al**. developed a gradient nanostructured surface layer on precipitation-hardened stainless steel using ultrasonic surface rolling. This treatment produced a refined surface microstructure with high compressive residual stress, leading to a significant improvement in fretting fatigue life and resistance to surface damage.

**[37] Dai and colleagues** investigated laser shock peening as a method to enhance rolling contact fatigue performance of stainless steel. Their experiments revealed that the induced compressive residual stresses and surface hardening generated by laser peening greatly improve fatigue durability.

**[38] Chen et al**. examined the low-cycle fatigue behavior of austenitic stainless steel intended for seismic applications. Their experimental study showed that the material exhibits high ductility and stable hysteresis loops, indicating excellent energy dissipation capacity under cyclic deformation.

**[39] Liu et al.** studied the fatigue response of duplex stainless steel with a gradient nanostructured surface layer produced using ultrasonic rolling. Their findings revealed that surface nanostructuring enhances high-cycle fatigue life but may reduce low-cycle fatigue resistance due to changes in deformation mechanisms.

**[40] Zulić and co-workers** demonstrated that laser shock peening significantly improves the fatigue performance of additively manufactured stainless steel by introducing beneficial compressive residual stresses and refining surface microstructure.

**[41] Several other researchers** have also reported that surface modification techniques such as shot peening, deep rolling, laser shock peening, micro-shot peening, and water jet peening can effectively enhance fatigue life by improving surface hardness, reducing surface roughness, and introducing compressive residual stress fields.

### 2.2 Literature Gap

While a substantial body of research exists on the tensile testing of steel, a persistent requirement remains to empirically assess widely utilized steel rods to confirm their mechanical characteristics under standardized conditions. This study aims to experimentally investigate the tensile performance of steel rods using a Universal Testing Machine and to compare the acquired data with established standard values.

### 2.3 Objectives

The primary objective of this research is to conduct an experimental investigation into the tensile performance of TIG-welded mild steel rods featuring different joint angles. The study to determine how various joint geometries affect the mechanical response of welded connections under tensile stress.

In this purpose, mild steel rod specimens were fabricated with joint angles of 0° (horizontal), 15°, 30°, and 45°. All joints were created using the Tungsten Inert Gas welding process under consistent parameters to ensure uniform weld quality. Tensile testing was performed on each welded specimen with a Universal Testing Machine to assess load-bearing capacity, deformation patterns, and fracture characteristics.

The load-displacement data collected is used to analyze the stress-strain behavior of the joints. The research specifically examines the influence of joint angle on tensile strength and ductility, pinpoints failure initiation sites, and investigates fracture mechanisms within the weld metal and heat-affected zone. The final aim is to identify the joint angle that yields the optimal tensile performance and structural reliability for welded mild steel components.

## CHAPTER 3
## METHODOLOGY

### 3.1 Workpiece Preparation

#### 3.1.1 Preparation of identical workpiece

For this experimental study, uniform mild steel workpieces were prepared to guarantee consistency in material properties and dimensional precision. Five mild steel rods of identical length approximately 1.5 feet each were sourced from the same stock batch to minimize variations in chemical makeup and mechanical behavior. A preliminary visual inspection confirmed the absence of surface flaws, cracks, or warping.

The central segment of each rod was machined via milling and turning operations to achieve a consistent cross-section appropriate for both welding and tensile testing. Surface finishing was subsequently applied to eliminate tool marks and irregularities, facilitating precise alignment during welding. Following machining, the rods were thoroughly cleaned to remove any contaminants such as oil, dust, or oxide layers, thereby promoting optimal weld penetration and fusion.

Each rod was then accurately marked at its midpoint and cut at the designated joint angles 0°, 15°, 30°, and 45°using suitable cutting tools. Meticulous attention was given to maintaining dimensional uniformity and angular accuracy

across all specimens. The prepared workpieces were then correctly aligned in preparation for TIG welding. This methodical preparation of identical samples ensured that the tensile test results would be dependable and directly comparable across the different joint configurations.

### 3.1.2 Raw Material Selection

At this stage, mild steel rods were chosen as the foundational material for the experimental procedure. The rods possessed a consistent diameter and were approximately 1.5 feet in length. Mild steel was selected for its superior weldability, good ductility, moderate strength, and extensive use in industry. A visual inspection was conducted on each rod to verify the absence of surface cracks, corrosion, warping, or other production flaws.

Only straight and defect-free rods were utilized for specimen fabrication to ensure consistency in the experimental outcomes

.

**Figure 3.1 Raw mild steel rods used for specimen preparation**

### 3.1.3 Machining of Rods

The chosen mild steel rods were machined on a lathe to create a uniform gauge section. This machining ensured all specimens had identical dimensions, which is crucial for obtaining accurate and comparable tensile test results. The process also produced a smooth, cylindrical surface essential for secure gripping in the Universal Testing Machine.

Following machining, a dimensional inspection was performed using a vernier caliper to verify the consistent diameter of each specimen.

**Figure 3.2 Machining of mild steel rod for specimen preparation**

### 3.1.4 Surface Finishing

Following the machining operation, surface finishing was carried out using emery paper. This step eliminated tool marks, burrs, and sharp edges left from the machining process. Achieving a smooth surface finish is critical, as rough surfaces can act as stress concentrators and potentially influence tensile test outcomes.
Furthermore, surface finishing enhances the precision of elongation measurements taken during the tensile test.

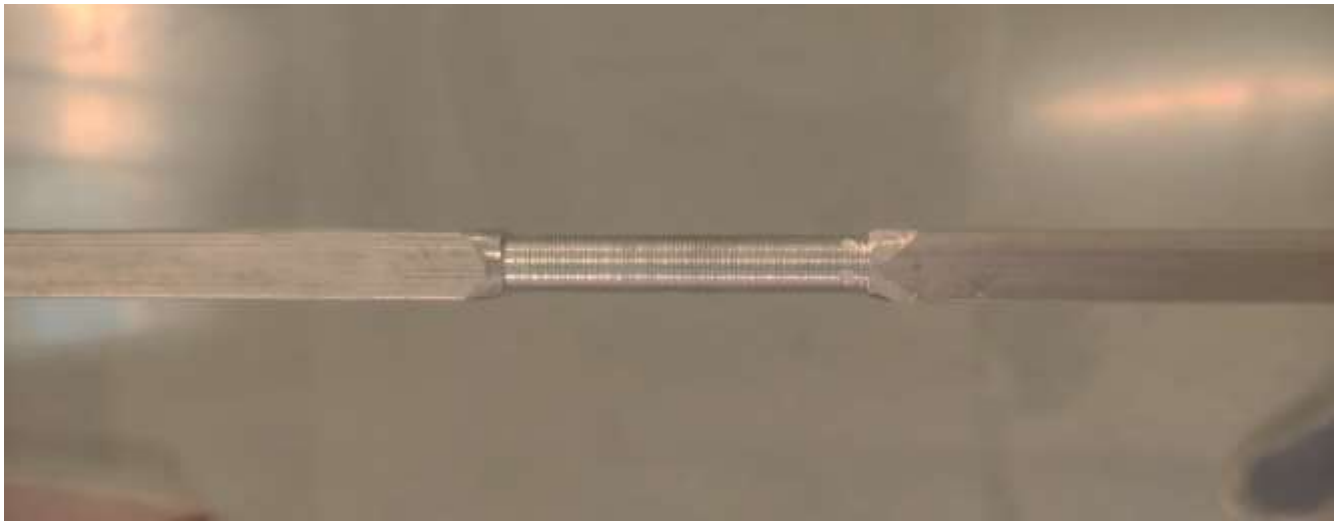

**Figure 3.3 Surface Finishing before TIG welding**

### 3.1.5 Cutting of Rods at Different Joint Angles

The rods were sectioned at their center point using a power cutting machine to create two equal halves for subsequent welding. This cutting was executed at five distinct joint angles: 0° (horizontal), 15°, 30°, and 45°. Prior to cutting, a protractor was used to mark each angle precisely, ensuring dimensional accuracy. The purpose of preparing these varied joint angles was to investigate the influence of joint inclination on the tensile strength and failure characteristics of TIG-welded connections.

### 3.1.6 Edge Preparation and Cleaning

Following the cutting process, the joint edges were readied for welding. The cut surfaces were lightly ground to eliminate sharp edges and to guarantee a proper fit-up between the pieces. A wire brushing operation was performed to strip away oxide layers and surface contaminants.

Subsequently, the joint surfaces were cleaned with acetone to remove any residual oil, grease, or dust. Clean surfaces are essential for producing a high-quality weld with adequate penetration and minimal defects.

### 3.1.7 Joint Alignment Before Welding

The two cut sections of each rod were carefully aligned using a welding jig. This fixture was essential for preserving the specified joint angle throughout the welding process and preventing any misalignment.

Proper alignment is critical, as any angular deviation can lead to eccentric or off-axis loading during the tensile test, which could compromise the accuracy of the results. The alignment was verified prior to welding to confirm the straightness of the assembly.

### 3.1.8 TIG Welding Process

TIG welding was applied to all specimens using consistent welding parameters. A tungsten electrode and argon shielding gas were employed to prevent oxidation during the process. The welding current, voltage, and gas flow rate were maintained at constant levels for every specimen to guarantee uniform weld quality.

The welding was executed with care to achieve complete penetration and a uniform weld bead profile. The torch was moved steadily along the joint path to ensure a consistent heat input throughout.

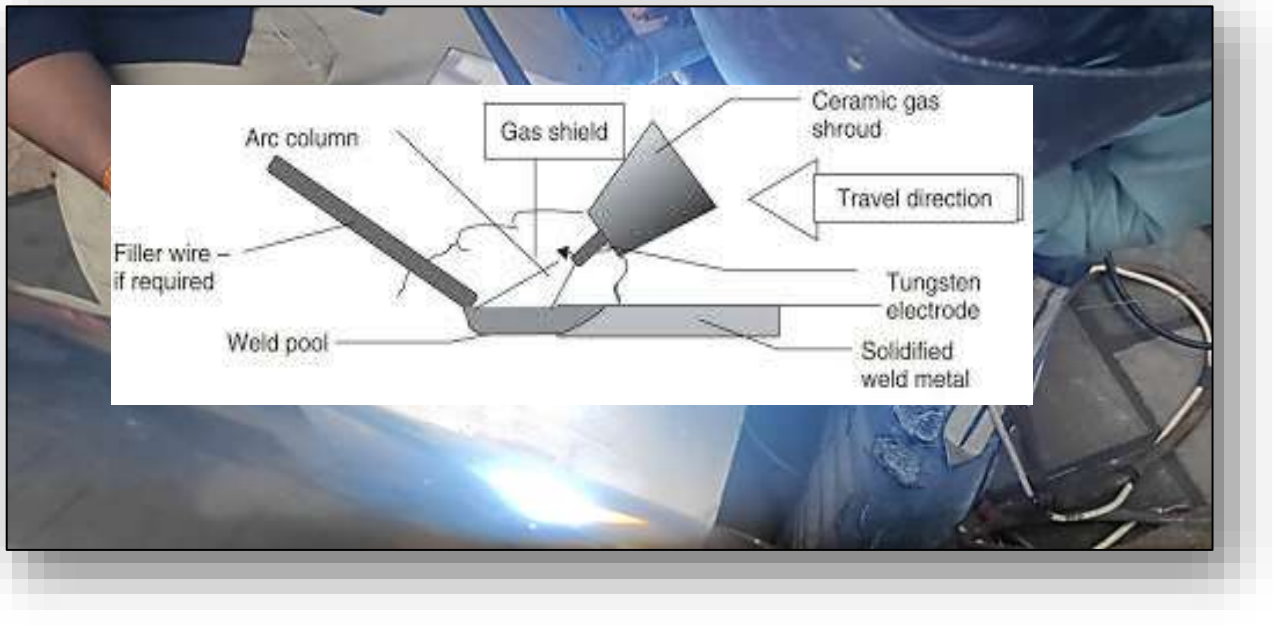


**Figure 3.4 TIG Welding Process**

### 3.1.9 Cooling and Post-Weld Cleaning

Following welding, the specimens were permitted to cool naturally to ambient temperature. Forced cooling methods were avoided to prevent the introduction of residual stresses that could compromise weld integrity.

After cooling, post-weld cleaning was performed using a wire brush to eliminate oxidation and surface contaminants from the weld bead.

### 3.1.10 Final Welded Specimens

Following the cooling and cleaning steps, the welded specimens underwent a visual inspection to detect any surface flaws, including cracks, porosity, or lack of fusion. Each specimen was clearly labeled with its corresponding joint angle to facilitate identification during subsequent tensile testing.
These final, prepared welded specimens were then ready for tensile evaluation on the Universal Testing Machine.

**Figure 3.5 TIG welded mild steel specimens (0°, 15°, 30°, and 45°)**

### 3.1.11 Tensile Testing on UTM

The welded specimen was securely clamped between the grips of the Universal Testing Machine. A gradually increasing load was applied, and the corresponding displacement was automatically recorded by the machine's data acquisition system. The test proceeded until the specimen fractured. The captured load-displacement data was subsequently used to

generate stress-strain curves and to analyze key properties such as tensile strength, ductility, and fracture characteristics.


**Figure 3.6 Tensile testing of welded specimen on Universal Testing Machine**

**3.2 Tensile Test of workpiece**

tensile testing was performed on all welded samples to assess their mechanical response under axial tensile stress. The tests were conducted using a Universal Testing Machine (UTM), which applies a progressively increasing force while simultaneously measuring the specimen's elongation. This method is standard for determining key properties like tensile strength, ductility, and fracture characteristics of materials and welded joints.

Each welded sample was carefully secured between the UTM's upper and lower grips, ensuring precise alignment with the loading axis to prevent bending or off-center forces. The gauge length was marked before testing to allow for accurate elongation measurement. A tensile load was then applied at a constant crosshead speed until fracture occurred. Throughout the test, the machine continuously recorded the load and corresponding displacement values.

The load-displacement data captured by the UTM was subsequently used to generate stress-strain curves for each specimen. These curves offered critical insights into the elastic behavior, yield point, plastic deformation, and ultimate tensile strength of the welded joints. Post-test examination focused on the fracture location and failure mode, with

specific attention paid to the weld metal and heat-affected zone. The tensile test results provided the foundational data for a comparative analysis of the tensile performance of TIG-welded mild steel rods across the different joint angles.

**Figure 3.6 Tensile testing of welded specimen (0°, 15°, 30°, and 45°)**

## CHAPTER 4
## RESULT AND DISCUSSION

### 4.1 Result

The experimental investigation establishes that the joint angle has a substantial impact on the tensile performance of TIG-welded mild steel rods. Specimens with lower joint angles demonstrated superior load distribution, greater ductility, and enhanced tensile strength. Conversely, higher joint angles led to diminished elongation and early failure, primarily caused by increased stress concentration within the weld region.

The results affirm that joint geometry is a critical factor, with lower angles promoting higher ductility and stable fracture through more uniform stress distribution. In contrast, higher angles induce premature failure due to the combined effects of shear and bending stresses, which become concentrated near the weld and the heat-affected zone (HAZ).

### 4.2 Load Displacement Result Tables

Based on the experimental data, the mechanical performance of the joints varies substantially with their orientation. The 0° joint displayed remarkable ductility, achieving the highest displacement (51.8 mm) and strain (10.36), and exhibited a clear yield plateau followed by extensive plastic deformation before failing at 285.70 MPa. The 15° joint attained the peak strength of 299.45 MPa with moderate displacement (21.3 mm) and balanced ductility (strain 4.26). In contrast, the 30° and 45° joints showed more brittle behavior, characterized by limited displacement (7.5 mm and 6.7 mm, respectively) and lower strain values (1.50 and 1.34), despite maintaining notable strength levels of 244.89 MPa and 233.16 MPa.

These findings demonstrate that joint orientation is a critical factor governing the strength-ductility balance. Lower angles offer superior deformation capacity, while specific intermediate angles (15°) can optimize strength performance.

**Table 4.1 Load -Displacement Data for Horizontal Specimen (0° Joint)**

| Load (KN) | Displacement (MM) |
|---|---|
| 00 | 00 |
| 0.270 | 0.7 |
| 4.238 | 1.1 |
| 3.210 | 3.2 |
| 3.150 | 6.2 |
| 3.160 | 9.1 |
| 3.170 | 12.2 |
| 3.180 | 15.5 |
| 3.360 | 42.2 |
| 3.710 | 43.1 |
| 4.230 | 44.8 |
| 7.100 | 46.6 |
| 10.720 | 47.5 |
| 25.510 | 49.9 |
| 31.250 | 50.6 |
| 32.320 | 51.8 |

**Table 4.2 Load -Displacement Data for 15° Joint**

| Load (KN) | Displacement (MM) |
|---|---|
| 00 | 00 |
| 0.890 | 0.3 |
| 3.420 | 1.8 |
| 3.220 | 4.3 |
| 3.210 | 6.9 |
| 3.330 | 9.5 |
| 3.400 | 12.0 |
| 4.090 | 14.3 |
| 6.420 | 15.8 |
| 9.300 | 16.6 |
| 14.180 | 17.6 |
| 21.199 | 18.7 |
| 31.440 | 19.7 |
| 33.880 | 21.3 |

**Table 4.3 Load -Displacement Data for 30° Joint**

| Load (KN) | Displacement (MM) |
|---|---|
| 00 | 00 |
| 4.490 | 0.6 |
| 4.890 | 2.1 |
| 7.880 | 3.5 |
| 15.340 | 5.2 |
| 25.190 | 6.5 |
| 27.680 | 6.9 |
| 27.700 | 7.5 |

**Table 4.4 Load -Displacement Data for 45° Joint**

| Load (KN) | Displacement (MM) |
|---|---|
| 00 | 00 |
| 0.430 | 0.3 |
| 1.070 | 0.5 |
| 3.610 | 0.7 |
| 3.920 | 1.0 |
| 4.490 | 1.7 |
| 5.090 | 2.3 |
| 5.990 | 2.9 |
| 6.700 | 3.1 |

| | |
|---|---|
| 7.340 | 3.4 |
| 9.940 | 4.1 |
| 10.200 | 4.2 |
| 11.200 | 4.4 |
| 12.270 | 4.7 |
| 13.400 | 4.9 |
| 15.340 | 4.9 |
| 15.390 | 5.2 |
| 16.600 | 5.4 |
| 18.560 | 5.7 |
| 20.700 | 6.0 |
| 24.280 | 6.4 |
| 26.370 | 6.7 |

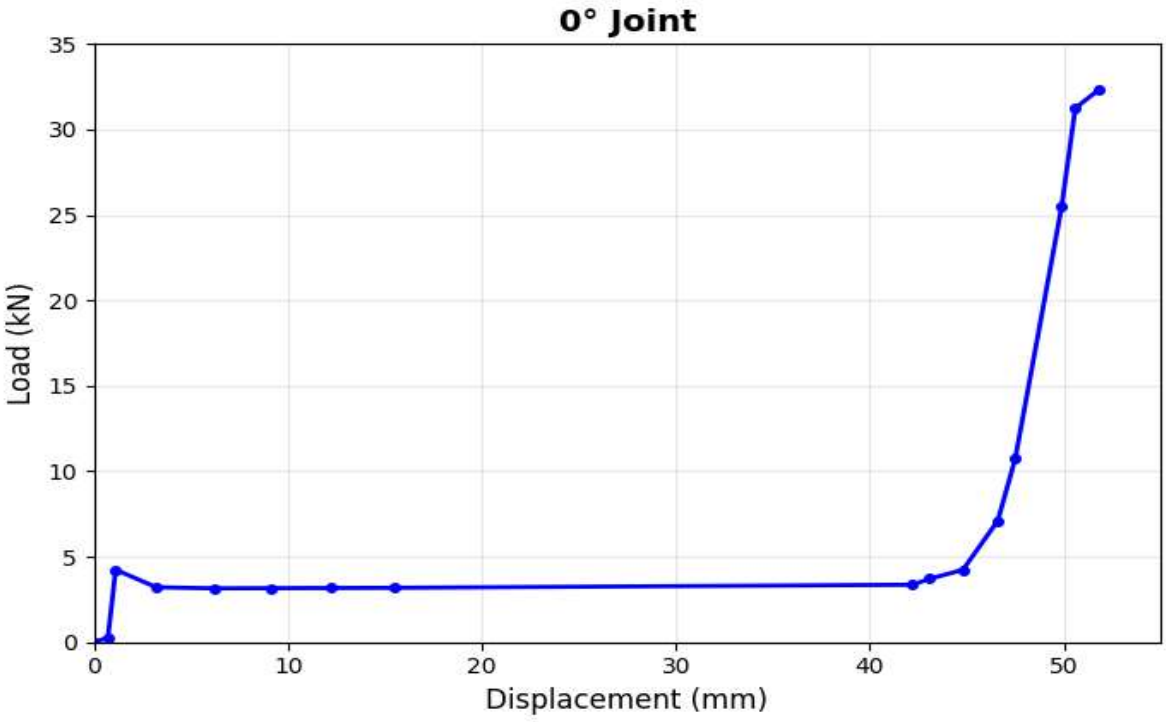


**Figure 4.1 Load -Displacement graph for 0° Joint**

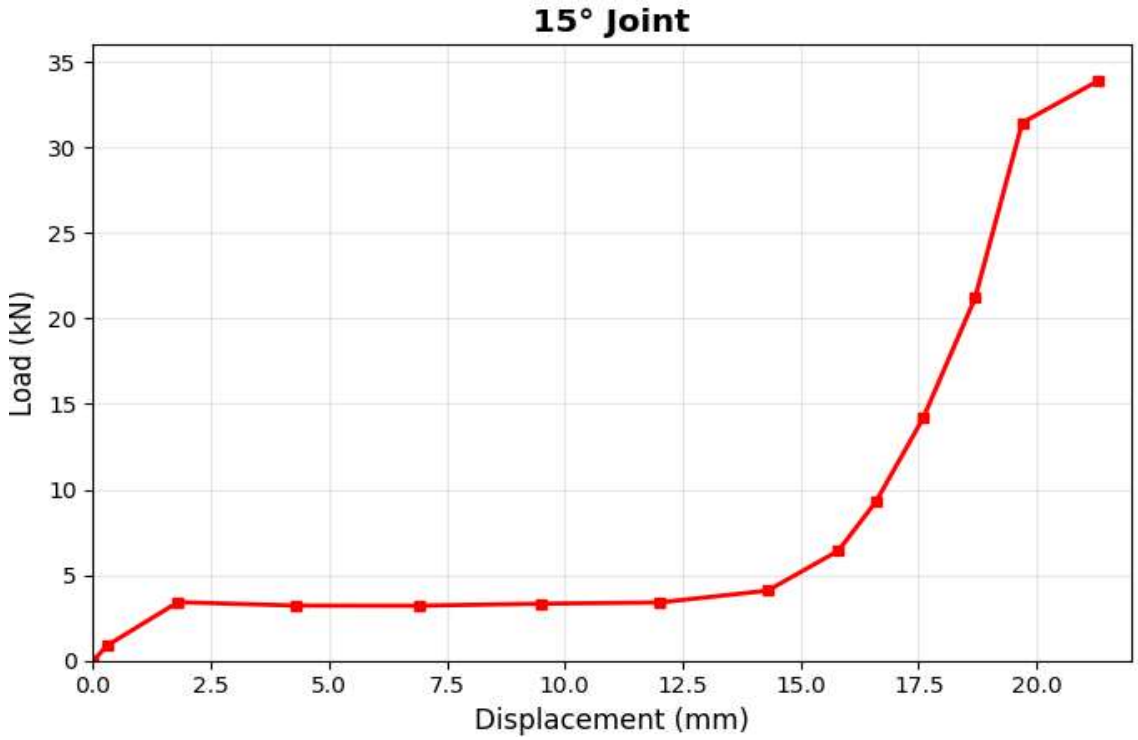


**Figure 4.2 Load -Displacement graph for 15° Joint**

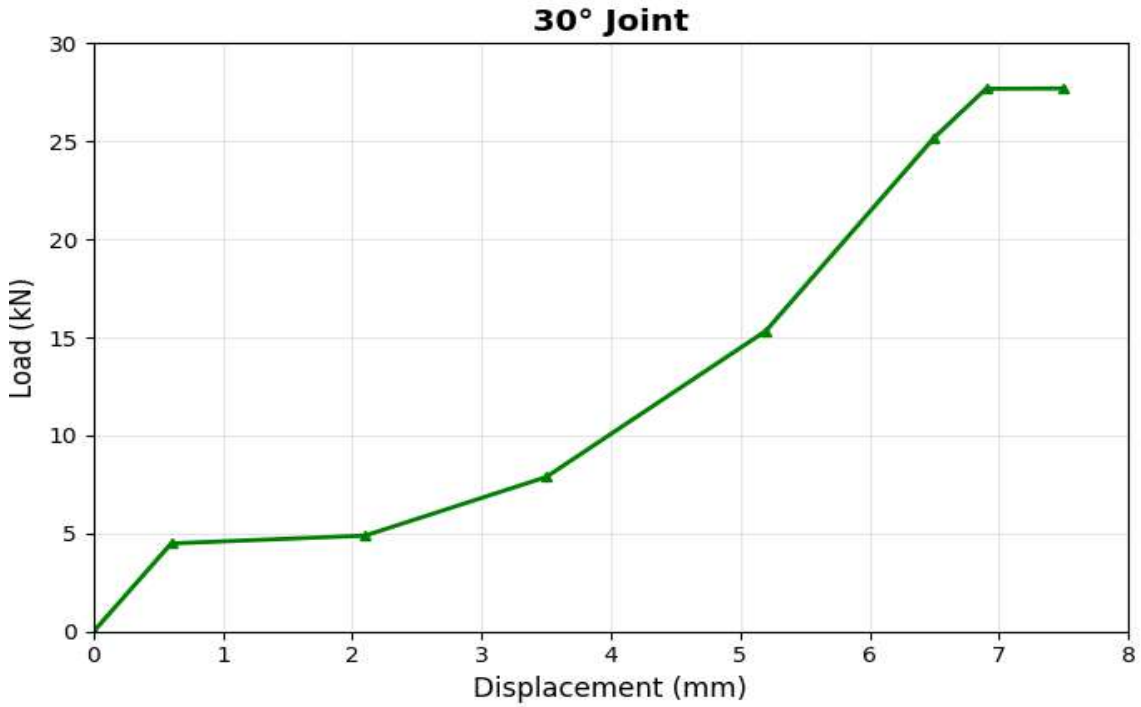


**Figure 4.3 Load -Displacement graph for 30° Joint**

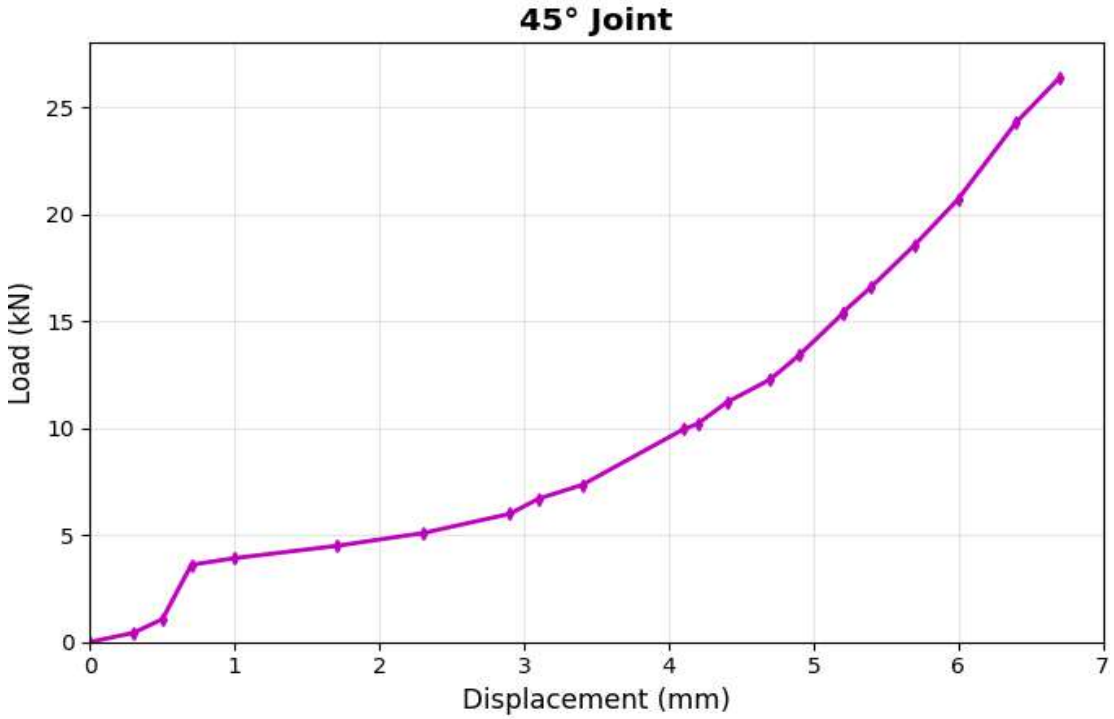


**Figure 4.4 Load -Displacement graph for 45° Joint**

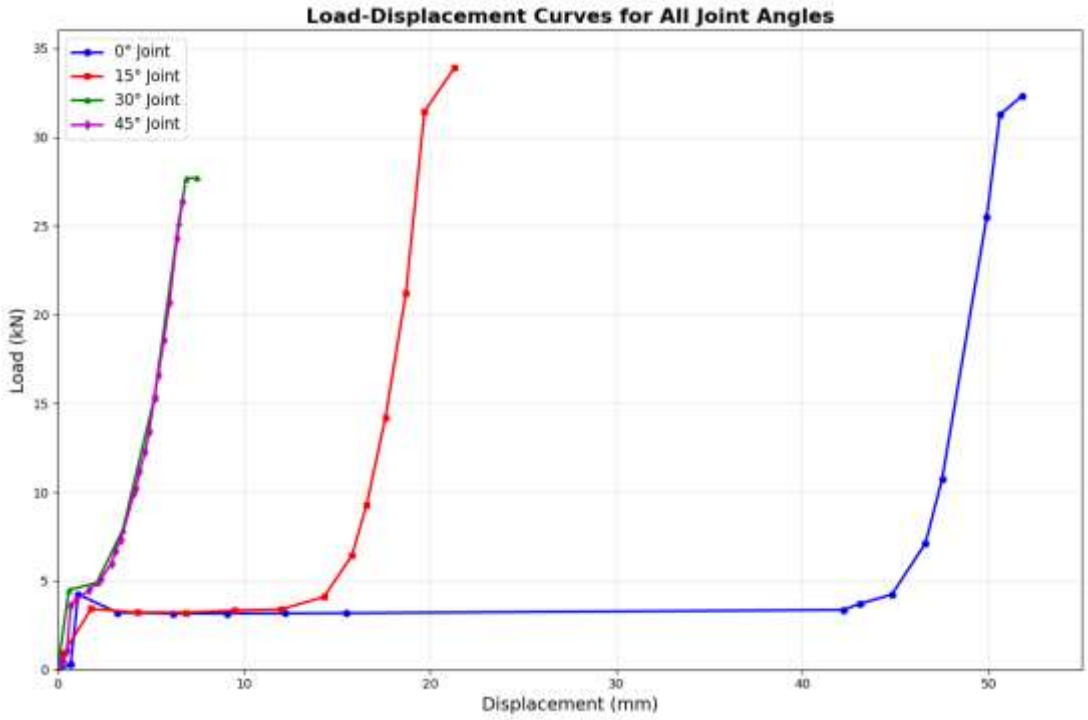


**Figure 4.5 Plot Comparative All Joint Angles Diagram**

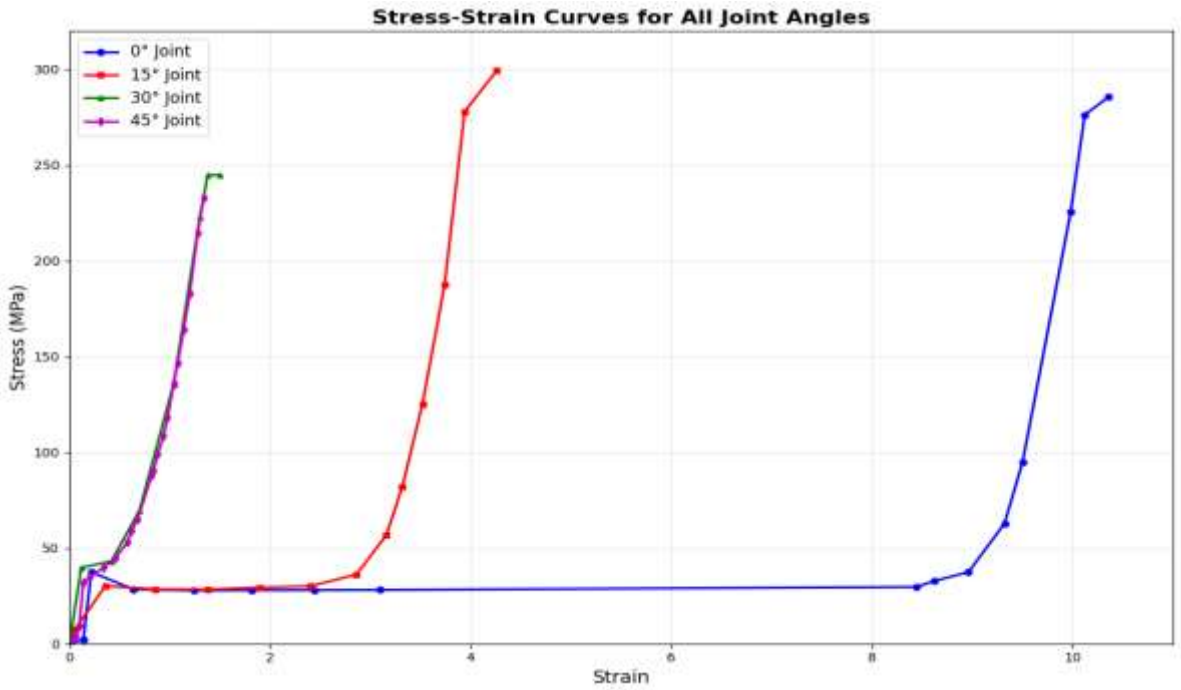


**Figure 4.6 Plot Comparative Stress Strain Diagram**

### 4.3 Stress and Strain Calculation

Stress and strain were computed using the standard formulas:

Stress (σ) in MPa = Applied Load (in Newtons) / Original Cross-sectional Area (in mm²)

Strain (ε)= Total Extension (in mm) / Original Gauge Length (in mm)

The relevant specimen dimensions were:

Dimeter(d) = 10mm

Gauge length ($L_o$) = 50mm

Cross-section Area($A_o$) = = $\pi \times d^2 / 4 = 78.5$ mm²

### 4.4 Stress–Strain Result Tables

**Table 4.5 Stress–Strain Data for Horizontal Specimen (0° Joint)**

| Load (KN) | Displacement (mm) | Stress (MPa) | Strain |
|---|---|---|---|
| 0.000 | 0.0 | 0.00 | 0.000 |
| 0.270 | 0.7 | 3.44 | 0.014 |
| 4.238 | 1.1 | 53.99 | 0.022 |
| 3.210 | 3.2 | 40.89 | 0.064 |
| 3.150 | 6.2 | 40.13 | 0.124 |
| 3.160 | 9.1 | 40.25 | 0.182 |
| 3.170 | 12.2 | 40.38 | 0.244 |
| 3.180 | 15.5 | 40.51 | 0.310 |
| 3.360 | 42.2 | 42.80 | 0.844 |
| 3.710 | 43.1 | 47.26 | 0.862 |
| 4.230 | 44.8 | 53.89 | 0.896 |

| | | | |
|---|---|---|---|
| 7.100 | 46.6 | 90.45 | 0.932 |
| 10.720 | 47.5 | 136.56 | 0.950 |
| 25.510 | 49.9 | 324.97 | 0.998 |
| 31.250 | 50.6 | 398.09 | 1.012 |
| 32.320 | 51.8 | 411.79 | 1.036 |

**Table 4.6 Stress–Strain Data for 15° Joint**

| Load (KN) | Displacement (mm) | Stress (MPa) | Strain |
|---|---|---|---|
| 0.000 | 0.0 | 0.00 | 0.000 |
| 0.890 | 0.3 | 11.34 | 0.006 |
| 3.420 | 1.8 | 43.57 | 0.036 |
| 3.220 | 4.3 | 41.03 | 0.086 |
| 3.210 | 6.9 | 40.89 | 0.138 |
| 3.330 | 9.5 | 42.42 | 0.190 |
| 3.400 | 12.0 | 43.31 | 0.240 |
| 4.090 | 14.3 | 52.10 | 0.286 |
| 6.420 | 15.8 | 81.78 | 0.316 |
| 9.300 | 16.6 | 118.47 | 0.332 |
| 14.180 | 17.6 | 180.64 | 0.352 |
| 21.199 | 18.7 | 270.05 | 0.374 |
| 31.440 | 19.7 | 400.64 | 0.394 |
| 33.880 | 21.3 | 431.82 | 0.426 |

**Table 4.7 Stress–Strain Data for 30° Joint**

| Load (KN) | Extension (mm) | Stress (MPa) | Strain |
|---|---|---|---|
| | | | |
| 0.000 | 0.0 | 0.00 | 0.000 |
| 4.490 | 0.6 | 57.23 | 0.012 |
| 4.890 | 2.1 | 62.34 | 0.042 |
| 7.880 | 3.5 | 100.38 | 0.070 |
| 15.340 | 5.2 | 195.41 | 0.104 |
| 25.190 | 6.5 | 320.70 | 0.130 |
| 27.680 | 6.9 | 352.42 | 0.138 |
| 27.700 | 7.5 | 352.67 | 0.150 |

**Table 4.8 Stress–Strain Data for 45° Joint**

| Load (KN) | Displacement (mm) | Stress (MPa) | Strain |
|---|---|---|---|
| 0.430 | 0.3 | 5.48 | 0.006 |
| 1.070 | 0.5 | 13.64 | 0.010 |
| 3.610 | 0.7 | 46.01 | 0.014 |
| 3.920 | 1.0 | 49.94 | 0.020 |
| 4.490 | 1.7 | 57.23 | 0.034 |

| | | | |
|---|---|---|---|
| 5.090 | 2.3 | 64.84 | 0.046 |
| 5.990 | 2.9 | 76.31 | 0.058 |
| 6.700 | 3.1 | 85.35 | 0.062 |
| 7.340 | 3.4 | 93.50 | 0.068 |
| 9.940 | 4.1 | 126.62 | 0.082 |
| 10.200 | 4.2 | 129.94 | 0.084 |
| 11.200 | 4.4 | 142.68 | 0.088 |
| 12.270 | 4.7 | 156.31 | 0.094 |
| 13.400 | 4.9 | 170.70 | 0.098 |
| 15.340 | 5.2 | 195.41 | 0.104 |
| 15.390 | 5.2 | 196.05 | 0.104 |
| 16.600 | 5.4 | 211.46 | 0.108 |
| 18.560 | 5.7 | 236.43 | 0.114 |
| 20.700 | 6.0 | 263.69 | 0.120 |
| 24.280 | 6.4 | 309.30 | 0.128 |
| 26.370 | 6.7 | 335.92 | 0.134 |

**4.5 Strain Stress Curve**

A stress-strain diagram is a plot that illustrates the correlation between stress and strain, derived from measurements taken in a tensile test. Stress is calculated by dividing the applied force by the initial cross-sectional area of the sample. Strain is determined as the ratio of elongation to the original gauge length.

The curve begins with a straight-line segment known as the elastic region. Within this phase, stress and strain exhibit a direct linear relationship, adhering to Hooke's Law. If the load is released during this stage, the material completely regains its initial shape and size, showing no residual deformation.

When the stress exceeds a specific threshold, called the elastic limit, the curve bends away from linearity, marking the start of the plastic region. Here, deformation becomes irreversible; the material retains a permanent change in shape after the load is removed. The onset of this permanent deformation is identified as the yield point.

Following yielding, the stress rises further until it attains its peak, known as the ultimate tensile strength (UTS). This represents the maximum stress the material can sustain. After the UTS, necking a localized narrowing of the cross-section initiates. As a result, the nominal stress decreases despite ongoing increases in strain, ultimately leading to fracture.

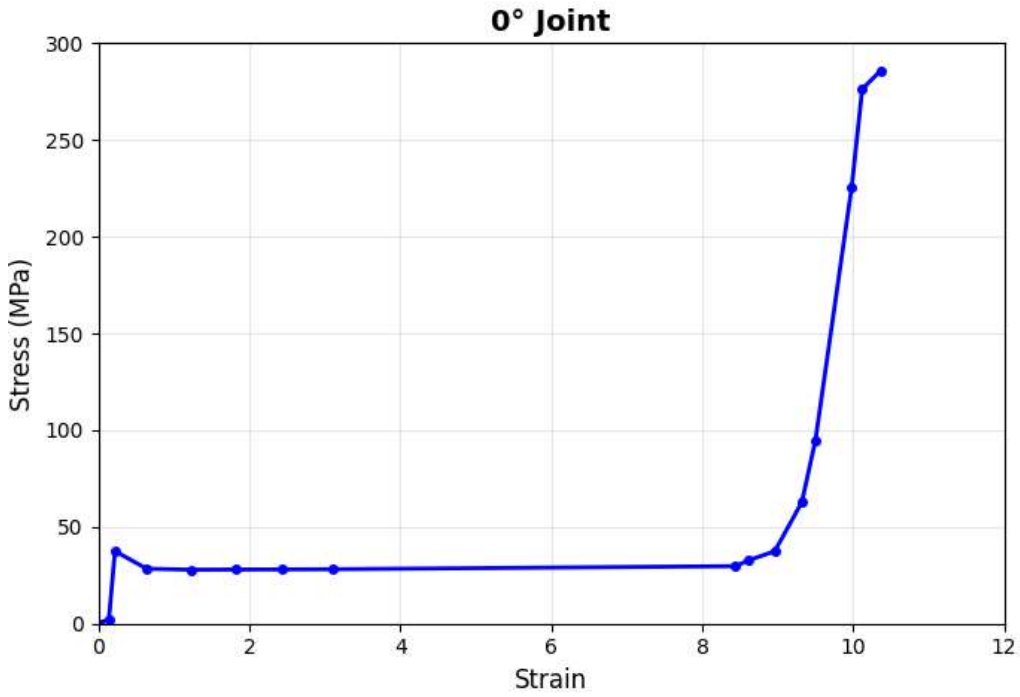


**Figure 4.7 Strain Stress Curve for Horizontal Specimen (0° Joint)**

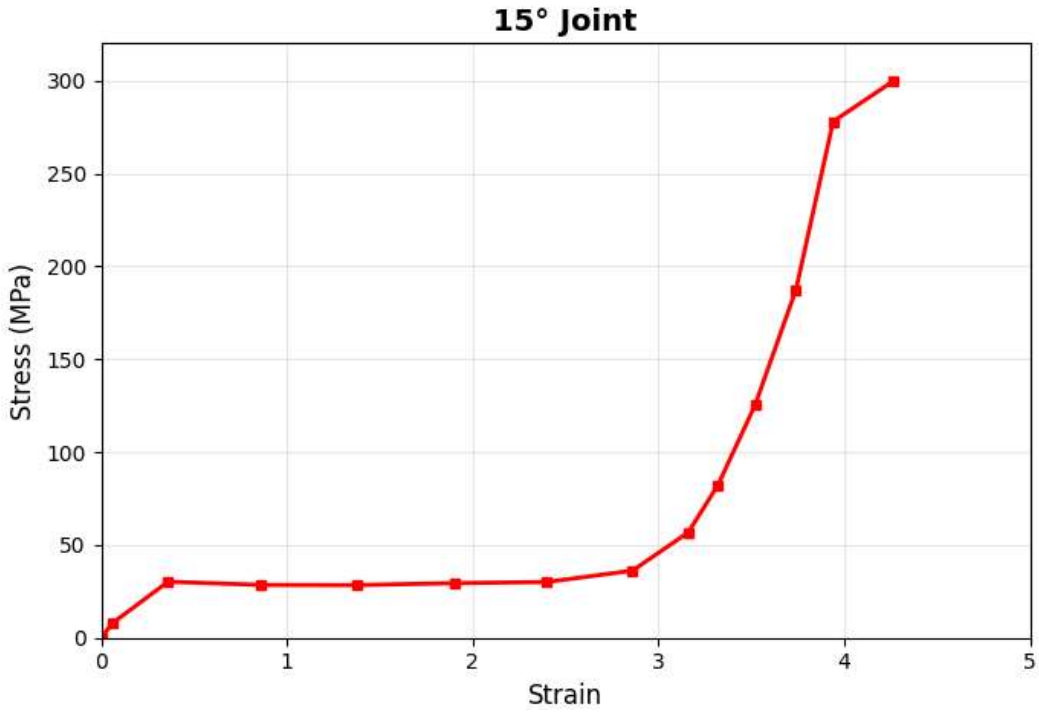


**Figure 4.8 Strain Stress Curve for 15° Joint**

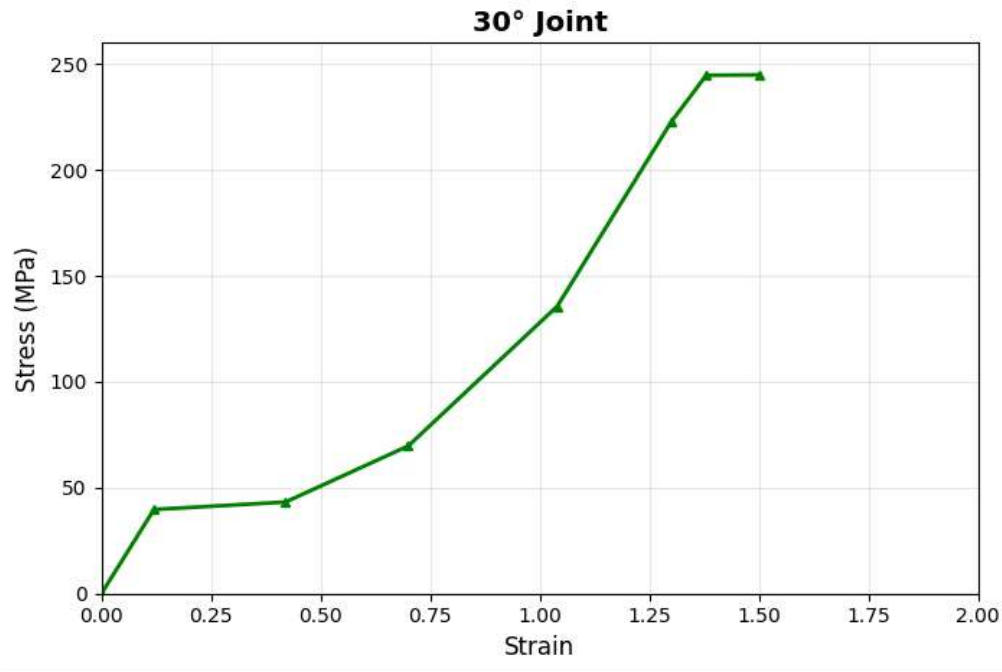


**Figure 4.9 Strain Stress Curve for 30° Joint**

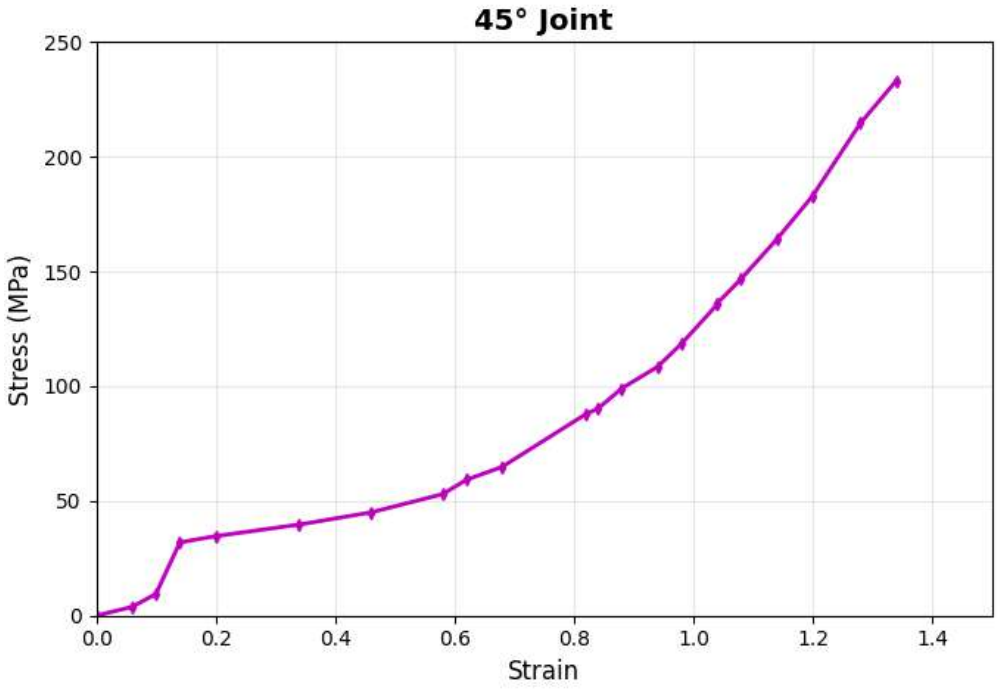


**Figure 4.10 Strain Stress Curve for 45° Joint**

### 4.6 Discussion of Results

The test outcomes clearly establish that the angle of the weld joint is a pivotal factor influencing the tensile response of TIG-welded steel rods.

The specimen featuring a 0° (horizontal) joint displayed superior performance, demonstrating the greatest ductility and

total extension prior to rupture. This behavior results from a direct axial load path and even stress distribution across the weld, effectively reducing localized stress peaks.

While the 15° joint retained considerable tensile strength with a minor decrease in ductility, a distinct pattern was observed as the joint angle grew to 30° and 45°. These configurations showed a continuous reduction in both their maximum tensile strength and their capacity for elongation.

This decline in mechanical properties at higher angles stems from an altered stress condition. Angled joints generate a mixture of tensile, shear, and bending stresses at the weld junction. This multifaceted stress field leads to pronounced localized stress concentrations, encouraging premature crack formation either in the weld material or the neighboring heat-affected zone (HAZ).

The uniform occurrence of failure adjacent to the weld zone verifies that the structural soundness of the weld metal and HAZ is the primary factor controlling the joint's total strength.

### 4.7 Failure Behavior

The consistent fracture of every specimen near the welded zone confirms that the weld metal and the heat-affected zone (HAZ) constitute the most vulnerable part of the assembled joint. In the case of angled joints, the initiation of fracture occurred more rapidly. This acceleration resulted from the addition of bending stresses to the main tensile force, which amplified localized stress concentrations and triggered failure at an earlier stage.

### 4.8 Summary

This study confirms that the geometry of the weld joint significantly affects tensile behavior. Joints with smaller angles, specifically 0° and 15°, offer an optimal balance of high strength and good ductility, rendering them appropriate for main structural roles. Conversely, joints with larger angles, such as 30° and greater, generate unfavorable stress conditions that diminish strength and encourage brittle fracture. Consequently, the application of these steeper angles should be restricted or excluded in the engineering of vital structural elements.

**Table 4.9 Comparative Results Table**

| Joint Angle | Max Load (KN) | Max Displacement (mm) | Behavior |
|---|---|---|---|
| 0° | 32.32 | 51.8 | Highly ductile |
| 15° | 33.88 | 21.3 | Strong & moderately ductile |
| 30° | 27.70 | 7.5 | Moderate |
| 45° | 26.37 | 6.7 | Brittle |

**Table 4.10 Maximum Load and Displacement**

| Specimen | Joint Angle | Maximum Load (KN) | Maximum Displacement (mm) |
|---|---|---|---|
| S1 | 0° (Horizontal) | 32.32 | 51.8 |
| S2 | 15° | 33.88 | 21.3 |
| S3 | 30° | 27.70 | 7.5 |
| S4 | 45° | 26.37 | 6.7 |

# CHAPTER 5
# CONCLUSION & FUTURE SCOPE

## 8.1 Conclusion

The experimental study on the tensile performance of TIG-welded mild steel rods, prepared with joint angles of 0°, 15°, 30°, and 45°, yields the following key conclusions:

- The angle of the welded joint is a decisive parameter influencing its tensile properties. The joint's geometry controls the pattern of internal stress distribution, which ultimately defines how much load the connection can support.
- Welds with smaller angles demonstrated enhanced mechanical characteristics. The 0° (horizontal) and 15° joints achieved both the maximum tensile strength and the highest ductility. This improved performance is linked to a more efficient transfer of force, which ensures better fusion and reduces localized stress build up.
- A clear inverse relationship existed between joint angle and tensile strength. Samples with 30° and 45° angles showed a significant drop in both strength and ability to elongate. This weakening is caused by a complicated interplay of tensile, shear, and bending stresses at the joint, increasing stress concentration and leading to early failure.
- For every specimen tested, fracture originated within the weld material or the nearby heat-affected zone (HAZ), regardless of the joint angle. This identifies these areas as the inherent weak links in the assembly when subjected to tensile forces.
- Although TIG welding created sound joints, their stress-strain response was critically dependent on orientation. The findings highlight a distinct compromise between strength and ductility: smaller angles support greater deformation, while larger angles, even when offering high strength (as with the 15° joint), reduce ductility and encourage brittle cracking.

## 8.2 Future Scope of Work

This investigation offers essential baseline information on the static tensile performance of TIG-welded joints at various angles. To build upon these results and increase their practical value for engineering, subsequent studies could pursue the following avenues:

- Analysis Under Fatigue and Dynamic Loads: Since structural elements in service often endure repetitive and impact loads, future research should assess the fatigue life and fracture toughness of these angled connections. Establishing the fatigue limit for each joint geometry is vital for ensuring the durability and reliability of designed components.
- In-Depth Microstructural Evaluation: A thorough microstructural investigation utilizing Scanning Electron Microscopy (SEM) and associated analytical techniques is advised. Such an examination would clarify the relationship between the joint angle, the associated thermal cycle, and the resultant microstructural changes in the weld metal and Heat-Affected Zone (HAZ). Insights into phase transformations, such as martensite development, and alterations in grain morphology would provide a mechanistic explanation for the measured variations in mechanical properties.
- Development of Numerical Models: Implementing Finite Element Method (FEM) simulations to replicate the tensile testing process would be advantageous. A validated computational model could forecast stress distributions, areas of plastic strain accumulation, and likely crack initiation sites for diverse joint angles. This serves as an effective predictive tool for refining weld designs prior to actual manufacturing.
- Optimization of Welding Process Parameters: A controlled experimental study that modifies primary welding variables including arc current, welding speed, and shielding gas type specifically for each joint angle could determine the ideal parameters to counteract the strength reduction observed at steeper angles. This would enable the direct application of research insights to enhance welding protocols.
- Exploration of Additional Materials and Joint Designs: Extending the research to incorporate other frequently joined materials, such as stainless steels or aluminium alloys, along with alternative joint geometries like single-V or double-V grooves, would foster a more comprehensive knowledge of how joint configuration influences the behaviour

of different materials.

**REFERENCE**

[1] Cruces, A. S., Lopez-Crespo, P., Bressan, S., & Itoh, T. (2019). Investigation of the multiaxial fatigue behaviour of 316 stainless steel based on critical plane method. *Fatigue and Fracture of Engineering Materials and Structures*, *42*(8), 1633–1645. https://doi.org/10.1111/ffe.12991

[2] Raghuwanshi, B. S., and Prakash, S., *Welding Technology*, McGraw Hill Education, New Delhi, India.

[3] Raghuwanshi, B. S., *Manufacturing Processes – Welding and Casting*, Dhanpat Rai Publications, New Delhi, India.

[4] Callister, W. D., and Rethwisch, D. G., *Materials Science and Engineering: An Introduction*, Wiley Publications.

[5] Dieter, G. E., *Mechanical Metallurgy*, McGraw Hill Education.

[6] Bansal, R. K., *Strength of Materials*, Laxmi Publications.

[7] Raghuwanshi, B. S., *Testing of Materials*, Dhanpat Rai Publications.

[8] ASTM E8/E8M – Standard Test Methods for Tension Testing of Metallic Materials, ASTM International.

[9] IS 1608:2005 – Metallic Materials – Tensile Testing at Room Temperature, Bureau of Indian Standards, New Delhi.

[10] ISO 6892 – Metallic Materials – Tensile Testing at Room Temperature, International Organization for Standardization.

[11] AWS D1.1 – Structural Welding Code (Steel), American Welding Society.

[12] Kumar, S., and Singh, R., "Experimental investigation of tensile strength of TIG welded mild steel joints," *International Journal of Mechanical Engineering*, 2021.

[13] Patel, A., and Verma, P., "Effect of joint angle on mechanical properties of welded steel joints," *International Journal of Engineering Research & Technology*, 2020.

[14] Sharma, V., and Mehta, N., "Mechanical behaviour of TIG welded mild steel specimens," *Journal of Manufacturing Processes*, 2019.

[15] Gupta, R., and Chaudhary, S., "Tensile testing and fracture analysis of welded steel joints," *International Journal of Advanced Mechanical Engineering*, 2022.

[16] Singh, A., and Kumar, P., "Study of heat affected zone in TIG welded mild steel," *Materials Today Proceedings*, 2023.

[17] Soyama, H., Chighizola, C. R., & Hill, M. R. (2021). Effect of compressive residual stress introduced by cavitation peening and shot peening on the improvement of fatigue strength of stainless steel. *Journal of Materials Processing Technology*, *288*, 116877. https://doi.org/10.1016/j.jmatprotec.2020.116877

[18] Yun, Z. O. U., Zhenkuan, S. A. N. G., Qilong, W. A. N. G., Tingchao, L. I., Dalei, L. I., & Yang, L. I. (2020). Improving the mechanical properties of 304 stainless steel using waterjet peening. *Materials Science*, *26*(2), 161–167.

[19] Kumar, P., Jayaraj, R., Suryawanshi, J., Satwik, U. R., McKinnell, J., & Ramamurty, U. (2020). Fatigue strength of additively manufactured 316L austenitic stainless steel. *Acta Materialia*, *199*, 225–239. https://doi.org/10.1016/j.actamat.2020.08.033

[20] Lai, W. J., Ojha, A., Li, Z., Engler-Pinto, C., & Su, X. (2021). Effect of residual stress on fatigue strength of 316L stainless steel produced by laser powder bed fusion process. *Progress in Additive Manufacturing*, 6(3), 375–383. https://doi.org/10.1007/s40964-021-00164-8

[21] Benchouia, S., Merakeb, N., Adjel, S., Ehlers, S., Baccouche, M., & Kaddour, A. (2019). Fatigue life enhancement of TIG-welded 304L stainless steels by shot peening. *International Journal of Advanced Manufacturing Technology*, *100*(9–12), 2885–2893. https://doi.org/10.1007/s00170-018-2898-5

[22] Braun, M., Mayer, E., Kryukov, I., Wolf, C., Böhm, S., Taghipour, A., Wu, R. E., Ehlers, S., & Sheikhi, S. (2021). Fatigue strength of PBF-LB/M and wrought 316L stainless steel: Effect of post-treatment and cyclic mean stress. *Fatigue and Fracture of Engineering Materials and Structures*, *44*(11), 3077–3093. https://doi.org/10.1111/ffe.13552

[23] Krovvidi, S. K., Goyal, S., & Bhaduri, A. K. (2019). Low cycle fatigue and creep-fatigue response of the 316Ti stainless steel. Frattura I. Strutturale (Ed.), 577–584.

[24] Jin, X., Ji, S., Liu, C., Shi, S., & Chen, X. (2020). Comparison of low cycle fatigue behavior of 304 stainless steels induced by tensile and torsional prestrain. *Fatigue and Fracture of Engineering Materials and Structures*, *43*(10), 2247–2258. https://doi.org/10.1111/ffe.13251

[25] de Abreu, M., Iordachescu, M., & Valiente, A. (2019). Influence of transversal loading on tensile and fatigue behaviour of high-strength lean duplex stainless steel wires. *Engineering Failure Analysis*, *102*, 417–424. https://doi.org/10.1016/j.engfailanal.2019.04.049